HHS Public Access

Author manuscript

J Biomed Mater Res A. Author manuscript; available in PMC 2024 September 01.

Published in final edited form as:

J Biomed Mater Res A. 2023 September ; 111(9): 1459–1467. doi:10.1002/jbm.a.37547.

Novel HALO® Image Analysis to Determine Cell Phenotype in Porous Precision-Templated Scaffolds

Nathan R. Chan[1,2], **Billanna Hwang**[3,4], **Rachel L. Waworuntu**[3], **An J. Tran**[3], **Buddy D. Ratner**[1,2,5], **James D. Bryers**[1,2]

[1]Molecular Engineering and Sciences Institute, University of Washington, Seattle, WA 98195, USA

[2]Department of Bioengineering, University of Washington, Seattle, WA 98195, USA

[3]Center for Lung Biology, University of Washington, Seattle, WA 98109, USA

[4]Department of Surgery, University of Washington, Seattle, WA 98195, USA

[5]Department of Chemical Engineering, University of Washington, Seattle, WA 98195, USA

Abstract

Image analysis platforms have gained increasing popularity in the last decade for the ability to automate and conduct high-throughput, multiplex, and quantitative analyses of a broad range of pathological tissues. However, imaging tissues with unique morphology or tissues containing implanted biomaterial scaffolds remain a challenge. Using HALO®, an image analysis platform specialized in quantitative tissue analysis, we have developed a novel method to determine multiple cell phenotypes in porous precision-templated scaffolds (PTS). PTS with uniform spherical pores between 30 and 40 μm in diameter have previously exhibited a specific immunomodulation of macrophages towards a pro-healing phenotype and an overall diminished foreign body response (FBR) compared to PTS with larger or smaller pore sizes. However, signaling pathways orchestrating this pro-healing in 40 μm PTS remain unclear. Here, we use HALO® to phenotype PTS resident cells and found a decrease in pro-inflammatory CD86 and an increase in pro-healing CD206 expression in 40 μm PTS compared to 100 μm PTS. To understand the mechanisms that drive these outcomes, we investigated the role of myeloid-differentiation-primary-response gene 88 (MyD88) in regulating the pro-healing phenomenon observed only in 40 μm PTS. When subcutaneously implanted in MyD88KO mice, 40 μm PTS reduced the expression of CD206, and the scaffold resident cells displayed an average larger nuclear size compared to 40 μm PTS implanted in mice expressing MyD88. Overall, this study demonstrates a novel image analysis method for phenotyping cells within PTS and identifies MyD88 as a critical mediator in the pore-size-dependent regenerative healing and host immune response to PTS.

Correspondence: James D. Bryers (3720 15th Ave NE, Seattle, WA 98105, USA. jbryers@uw.edu), Billanna Hwang (850 Republican Street, Seattle, WA 98109, USA. bhwang@uw.edu).

Conflict of Interest

The authors declare that there is no conflict of interest. Dr. Ratner is a founder and board member of Healionics, a clinical-stage Seattle-based company developing proprietary STAR® (Sphere Templated Angiogenic Regeneration) biomaterial scaffolds.

Keywords

biomaterial scaffolds; foreign body response; cell phenotype; macrophage polarization; MyD88

Introduction

With the advancement of high-resolution imaging and extraordinary growth made in the field of machine learning, image analysis platforms have become increasingly popular for delivering scalable, reproducible, and easy-to-use algorithms. The ability to automate and conduct high-throughput, quantitative image analysis has vastly improved current histopathology workflows and provided researchers with a plethora of extensive analytics. Reports have shown the application of image analysis algorithms for cell phenotyping[1], spatial analysis[2], and tissue classification[3] in cancer microenvironments[4,5] and pathological tissue[6]. Despite the widespread use of automated image analysis platforms, tissues with unique morphology or containing implanted biomaterials remain a hurdle.

Hydrogels are highly versatile scaffolding materials used in tissue engineering applications to promote tissue formation and repair. Scaffolds play an important role in regenerative medicine by providing an artificial 3D extracellular matrix (ECM)-like structure and microenvironment to support cellular activities such as infiltration, adhesion, proliferation, and differentiation. Additionally, hydrogel scaffolds can easily be manufactured with specific architectures to generate an immunomodulatory biomaterial capable of promoting biological integration, reducing fibrosis, and increasing vascularization[7,8]. Specifically, we have developed a porous precision-templated scaffold (PTS) platform where every pore and interconnect diameter are adjustable, uniform, and precisely controlled (narrow size distribution) throughout the scaffold. Independent of the polymer used, PTS with uniform, interconnected 40 μm pores uniquely demonstrate remarkable healing outcomes and an overall reduction in the foreign body response (FBR) while PTS of smaller or larger pore size exhibit minimal vascularization and a classic FBR[9–12]. Despite the favorable healing outcomes observed in 40 μm PTS, a better understanding of the FBR and the host immune responses are required to fully characterize the pro-healing, pore-size mediated phenomenon seen within 40 μm PTS.

Cell phenotyping remains a significant hurdle in deciphering the interaction between PTS and the host immune response. Image analysis algorithms for cell phenotyping have been minimally applied to biomaterial scaffolds; however, there is increasing demand for these data for use in a clinical setting to evaluate the biomaterial scaffolds as a potential therapeutic. Although manual assessment by trained pathologists remains the gold standard, the scoring of large data sets is limited by lengthy turnaround times. Therefore, the development of new technology and techniques to analyze pathological samples is required.

As a result, several studies have utilized HALO® as an easy-to-use, scalable digital pathology analysis platform to identify and quantify histopathological findings in tissues[2,5,6] and biomaterial scaffolds[13–16]. HALO® contains several functionalities that allow for tissue classification and the analysis of both cell expression and morphological data. Analysis of nuclear morphology in porous scaffolds presents a novel characterization

method and has been shown to directly translate to differences in gene expression through mechanotransduction[17]. Furthermore, analytics are provided on a cell-by-cell basis allowing for the quantification of spatial interactions and the investigation into how single cells contribute to the overall cell population. The application of a HALO® image analysis to phenotype and understand PTS resident cell populations provides immense value to move to clinical applications, and supplements transcriptomic and other molecular biology analytical techniques. Furthermore, expanding the use of HALO® to investigate signaling pathways provides additional understanding of mechanisms associated with PTS outcomes.

Within biomaterial scaffolds, toll-like receptor (TLR) signaling has emerged as a potential regulator of the inflammatory FBR. TLRs are a class of membrane-bound pattern recognition receptors (PRRs) that activate leukocytes in response to damage (DAMPs) and/or pathogen-associated molecular patterns (PAMPs). Activation of TLR signaling pathways is essential to the host immune response as it detects pathogens, initiates the production of inflammatory cytokines, and bridges innate and adaptive immunity[18,19]. TLR signaling is mediated by two major intracellular signaling pathways utilizing different adaptor proteins – myeloid-differentiation-primary-response gene 88 (MyD88) and toll/IL-1 receptor-domain-containing adapter-inducing interferon-β (TRIF). MyD88 plays a pivotal role in nearly all TLR immune cell activation (except for TLR3) and is responsible for mediating the transcription of pro-inflammatory cytokines such as IL-1, IL-6, and TNF-α inflammatory responses upon the activation of nuclear factor kappa B (NF-κB)[19,20]. In the context of biomaterial scaffolds, MyD88-mediated inflammation was identified as a contributing factor in the pro-fibrotic response to poly(ethylene glycol) hydrogels[21] while in electrospun scaffolds of varying fiber and pore sizes, MyD88-dependent signaling was implicated in pro-inflammatory M1-like macrophage polarization[22]. Together, a growing body of evidence highlights MyD88 as a potential mediator in the host immune cell response to biomaterial scaffolds. Therefore, we hypothesize that the regenerative healing found only in 40 μm PTS is dictated by MyD88-dependent signaling.

In this study, we apply a HALO® image analysis algorithm for cell phenotyping to investigate the potential role of MyD88 in regulating the unique pro-healing response observed in 40 μm PTS implants. Using HALO®, we provide novel quantitative profiling of macrophage (CD86, CD163, CD206) and T cell (CD3) populations and characterize the nuclear morphology of cells within 40 μm and 100 μm PTS. To further elucidate the role of MyD88-dependent wound healing observed in 40 μm PTS, surface marker expression in MyD88KO mice was compared in 40 μm and 100 μm PTS. Findings from this study will aid in the development of a comprehensive phenotyping approach to enhance understanding of the host immune response to implanted biomaterials.

Materials and Methods

Poly (2-hydroxyethyl methacrylate) (pHEMA) Scaffold Synthesis

While 40μm PTS exhibit remarkable healing regardless of the polymer employed, here we elect to use poly(2-hydroxyethyl methacrylate) due to its superior performance in histological sectioning. Porous precision-templated scaffolds (PTS) were fabricated as previously described using a patented sphere-templating method (Patent

US2008/0075752A1)[9–12]. Briefly, poly (methyl methacrylate) (PMMA) beads of 40 μm and 100 μm in diameter (Dynoseeds TA-40 and TA-100, respectively) were purchased from Microbeads AS (Skedsmokorset, Norway). A mold was created by forming a rectangular gasket by placing 0.8 mm thick Teflon tape strips (5 mm wide) on the outer edges of a 75 mm (L) 00D7 25 mm (W) 00D7 1 mm thick glass slide. Beads of desired size (40 or 100 μm) were poured into the recess formed by the tape strips, then a second glass slide is placed on top and clamped together. The mold was then agitated for 2 hours in a water bath sonicator followed by heating in an oven (Binder FP115UL-120V) to sinter the beads at their contact points, forming a 3D interconnected lattice structure. Oven sintering temperatures and times were optimized to achieve an interconnect diameter to pore diameter ratio between 25–33% by heating at 177°C for 25.5 hours (40 μm) or 169°C for 26 hours (100 μm). pHEMA precursor solution was formulated by mixing 5.1 mL 2-hydroxyethyl methacrylate (HEMA) (Polysciences), 0.24 mL tetraethylene glycol dimethacrylate (TEGDMA) (Polysciences), 1.5 mL ethylene glycol, 2.1 mL deionized water, and 20 mg 2,2-dimethoxy-1,2-diphenylethan-1-one (Irgacure 651) (BASF, Freeport, LA). The HEMA monomer solution was infiltrated into the mold with the sphere template and degassed under a vacuum. Broad-spectrum UV was used to cross-link the HEMA monomer solution into pHEMA via free-radical polymerization. The sphere template surrounded by pHEMA was removed from the glass mold and immersed in acetone to dissolve the PMMA beads. Resultant pHEMA PTS were sterilized in 70% ethanol and rehydrated in ultrapure water. PTS were cut into 6 mm round, 0.8 mm thick disks using a biopsy punch and lyophilized for storage.

Lyophilized scaffolds were characterized by scanning electron microscopy (SEM) and ImageJ software (NIH) to ensure scaffold interconnect to pore ratios were tightly controlled between 25–33%. Samples were sputter-coated for 120s with gold/palladium (NanoImages MCM-200) and then imaged on a scanning electron microscope (NanoImages SNE-3200M) at 5 kV with a 1 mm working distance. Before use, scaffolds were rehydrated in 1X pH 7.4 phosphate-buffered saline (PBS).

Mice

All animal experiments followed federal guidelines, and protocols were approved by the University of Washington Institutional Animal Care and Use Committee (Animal Welfare Assurance #A3464–01). G6.129P2-Lyz2$^{tm1(cre)lfo}$/J (LysM-Cre), B6.129(Cg)-Gt(ROSA)26Sor$^{tm4(ACTB-tdTomato,-EGFP)Luo}$/J (mTmG), and B6.129P2(SJL)-Myd88$^{tm1.1Defr}$/J (MyD88KO) mice were purchased from The Jackson Laboratory (Bar Harbor, ME). LysM-Cre:mTmG double transgenic mice for myeloid characterization were generated by crossing LysM-Cre mice with mTmG mice, as described previously[11,12], producing a reporter mouse strain in which cells of the myeloid lineage express green EGFP and all other cells express red tdTomato. Mice were housed in a pathogen-free facility at the University of Washington Department of Comparative Medicine.

Surgical scaffold implantation/harvest procedure

PTS implantations were performed in 6–8 week old male or female LysM-Cre:mTmG mice and MyD88KO mice. Briefly, mice were anesthetized with 2% isoflurane, the dorso-lumbar

region was shaved, and the skin was sterilized with three alternating betadine and 70% ethanol washes. A 1 cm long dorsal midline incision was made, and two subcutaneous pockets were formed, one on each side of the incision. Each pocket was implanted with one pHEMA scaffold (6 mm diameter, 0.8 mm thick), and the incision was closed with wound clips. One and two weeks after implantation surgery, scaffolds were excised and embedded in 0.7 × 0.7 cm disposable base molds with OCT compound (Tissue-Tek Sakura), and snap-frozen using liquid nitrogen.

Immunofluorescence Staining

OCT embedded PTS were cut on a cryotome (Leica CM1850) into 5 μm thick tissue sections and serial sections were placed on positively charged microscope slides. Samples were allowed to reach room temperature, followed by fixation in 10% neutral buffered formalin (BBC Biochemical). Endogenous peroxidases were blocked using 3% hydrogen peroxide, and cells were permeabilized with 0.1% Triton X-100 (Sigma-Aldrich). Washes with PBS were performed between each step. Non-specific binding was blocked using a solution consisting of 10% equine serum, 5% canine serum, and 1% bovine serum albumin in PBS for 1 hour at room temperature. Samples were washed with PBS and each section was individually stained with a 1:100 dilution of unlabeled primary antibody for either CD3 (Clone: 145–2C11, Invitrogen), CD86 (Clone: GL1, Invitrogen), CD163 (Clone: ED2, Bio-Rad), or CD206 (Clone: MR5D3, Invitrogen) at room temperature for one hour. Each primary antibody staining was performed on separate but serial histology sections from the same explanted PTS. As this study is preliminary, simultaneous staining with CD3, CD86, CD163, and CD206 primary antibodies on the same explanted PTS was not performed. Slides were incubated with Alexa Fluor® 750 (AF750, 1:200, Invitrogen) secondary antibody at room temperature for 1 hour and washed with PBS. PTS sections were cleared using Histo-Clear II (National Diagnostics), mounted using ProLong Gold Antifade Mountant with DAPI (Invitrogen), and covered with a #1.5 coverslip.

Image analysis

Images were acquired using the EVOS FL Color Imaging System equipped with the DAPI, GFP, Invitrogen Texas Red, and Invitrogen Cy7 EVOS LED light cubes (ThermoFisher) (Supplemental Table S1). Quantitative analysis of acquired images was performed using the CytoNuclear FL v1.4 algorithm in the HALO® image analysis software (Indica Labs; Albuquerque, NM) to simultaneously detect multiple positive fluorescence markers in the cytoplasm and nucleus of individual cells. Parameters in the CytoNuclear FL v1.4 algorithm were optimized through systematic variation and the real-time tuning function to remove auto-fluorescence detection and adjust for fluorophore brightness (Supplemental Table S2). The parameter settings in the CytoNuclear algorithm were verified by manual visual inspection of positive cells from randomly selected images. Four fluorescent colors were used in the image analysis of PTS explanted from LysM-Cre:mTmG mice. AF750 staining identified the marker of interest (CD3, CD86, CD163, or CD206) using the Cy7 filter, EGFP was expressed by cells of the myeloid lineage using the GFP filter, tdTomato was found in non-myeloid cells using the Texas Red filter, and DAPI was used as a nuclear counterstain. Data are reported as the total number of positive fluorescent events ($AF750^+$, $EGFP^+$, $tdTomato^+$, or $DAPI^+$) for each cell as well as the area and perimeter of DAPI-stained nuclei.

Specific phenotypes were defined using colocalization of multiple fluorescent markers to identify CD3 T lymphocytes, M1-like CD86 macrophages, or M2-like CD163 or CD206 macrophages. As CD3, CD86, CD163, and CD206 staining were performed on separate but serial sections from the same explanted PTS, the colocation of these markers was not performed. PTS explanted from MyD88KO mice were analyzed using only two fluorescent stains to determine the percentage of cells ($DAPI^+$) expressing CD3, CD86, CD163, or CD206 ($AF750^+$). Nucleus area and perimeter were also quantified from DAPI staining to determine morphological characteristics attributed to scaffold resident cells.

Statistical Analysis

Data are presented as mean ± 95% confidence interval. Graphical representation of data is expressed in boxplots, where the bottom and top of the box contain the first and third quartiles, respectively, with a vertical line through the median. Red diamonds denote values greater than 1.5 times the interquartile range (IQR), and whiskers represent the minimum and maximum data point excluding values greater than 1.5 00D7 IQR. Statistical analysis was performed using R Statistical Software (version 4.0.2) and the DescTools, MASS, stats, and qqplotr packages. Normality was determined for all sample groups using quantile-quantile (q-q) plots and the Shapiro-Wilks test with $\alpha = 0.05$. Non-parametric data were transformed using a Box-Cox transformation to satisfy the normality assumption in statistical tests. To determine statistical significance, Welch's t-test was performed for comparisons between two sample groups, and a one-way ANOVA with Dunnett's multiple comparison test was used for comparison with more than two sample groups. A p-value less than or equal to 0.05 was defined as statistically significant.

Data availability

The main data supporting the results in this study are available within the paper and its supplementary information. The raw and analyzed datasets generated in this study are available from Mendeley Data at doi: 10.17632/s94bpctvvr.1

Results

PTS pore size effects on resident cell phenotypes

To evaluate the phenotypes as a function of pore size, PTS with 40 μm pores or 100 μm pores were implanted subcutaneously into LysM-Cre:mTmG mice (40 μm PTS and 100 μm PTS, respectively) (Figure 1A) and explanted one or two weeks post-implantation. Scaffolds were analyzed by HALO® using the total number of cells expressing either CD3 (T lymphocytes), CD86 (M1-like macrophages), CD163 (M2-like macrophages), or CD206 (M2-like macrophages) per image area by immunofluorescence. In addition, a CytoNuclear FL algorithm was specifically designed to quantify and phenotype the cells within the PTS. Parameters in the CytoNuclear FL algorithm were optimized using systematic variation and the real-time tuning function to accurately detect single nuclei (based on nuclear contrast, intensity, size, roundness, and segmentation) and to adjust for fluorophore brightness and biomaterial auto-fluorescence.

At one week post-implantation, both the 40 μm PTS and the 100 μm PTS shared no differences in the total number of resident cells (1102 ± 218 cells per mm^2 image area in the 40 μm PTS, and 1001 ± 209 cells per mm^2 image area in the 100 μm PTS) (Figure 2A). After two weeks post-implantation, 40 μm PTS appear to contain a greater number of resident cells (1176 ± 378 cells per mm^2 image area) compared to 100 μm PTS (837 ± 90 cells per mm^2 image area), though not significant ($p = 0.053$). LysM-Cre:mTmG mice were used to fluorescently track myeloid lineages using a membrane-bound EGFP (green) while non-myeloid cells expressed tdTomato (red). No significant differences assessed by EGFP were observed between the 40 μm PTS and the 100 μm PTS at either one or two weeks post-implantation (Figure 2B).

To further characterize the cell populations within the PTS, the expression of CD3, CD86, CD163, or CD206 was performed on serial explanted scaffold sections. PTS with 100 μm pores demonstrated a statistically significant increase in the inflammatory marker CD86 at one week post-implantation compared to 40 μm PTS ($p = 0.046$, Figure 3C). In contrast, 40 μm PTS expressed an increase in CD206 expression at two weeks post-implantation ($p = 0.022$, Figure 3E). No significant differences were observed in CD3 or CD163 expression between any of the groups or time points (Figure 3BD). Together, these results demonstrate the role of scaffold resident cells from 100 μm PTS to induce a greater CD86 inflammatory response, while 40 μm PTS appears to produce an M2-like CD206 regenerative phenotype.

MyD88 signaling involved in pro-healing mechanisms seen in 40 μm PTS

We evaluated the involvement of MyD88-dependent signaling by implanting 40 μm PTS into MyD88KO mice (Figure 1B). Implantation of 100 μm PTS into MyD88KO mice was not performed as mice deficient in MyD88 have previously been established to impair wound healing[23]. Broad profiling of cell populations was performed using CD3 (T lymphocytes), CD86 (M1-like macrophages), CD163, or CD206 (M2-like macrophages).

Knockout of MyD88 did not affect the total number of cells within the 40 μm PTS implanted in MyD88KO mice. At one week post-implantation, an average of 973 ± 552 total cells per mm^2 image area were observed, and at two weeks post-implantation, there were 1366 ± 362 cells per mm^2 image area (compared to 1102 ± 218 cells per mm^2 image area at one week and 1176 ± 378 cells per mm^2 image area at two weeks post-implantation for 40 μm PTS implanted in LysM-Cre:mTmG; Figure 2A). From scaffold tissue sections explanted at one and two weeks, CD206 expression was significantly decreased in 40 μm PTS implanted in MyD88KO mice compared to 40 μm PTS implanted in LysM-Cre:mTmG mice ($p < 0.001$ and $p = 0.040$, respectively; Figure 3E). Despite decreases in M2-like CD206 expression, no changes were observed in CD163 expression, another marker associated with the M2-like phenotype (Figure 3D). This suggests that the pro-healing and pro-regenerative phenotype in 40 μm PTS arises through the activation of a MyD88-dependent pathway causing an increase in CD206 expression but not CD163. Within the MyD88KO mice, no significant change in CD3 or CD86 expression was observed (Figure 3BC). However, CD86 expression appears to decrease at two weeks post-implantation, but further study is required to confirm the overall trend. Taken together, these results highlight the importance of the CD206 positive phenotype in developing a pro-healing, regenerative 40 μm PTS.

Both pore size and MyD88 demonstrate unique nuclear size and morphology in scaffold environment

PTS consist of several interconnected pores generating a network of tight junctions through which cells must migrate. Scaffold architecture and surface topography are factors that contribute to the PTS microenvironment; however, the effect on cell morphology remains uncharacterized. Morphological characteristics were quantified from the immunofluorescence images based on DAPI staining of nuclei and detection by the CytoNuclear FL image analysis algorithm (Figure 4). Nucleus area and nucleus perimeter were measured values determined by image analysis. As a function of pore size, the mean nuclei area from cells resident in 40 μm PTS were smaller compared to cells resident in 100 μm PTS ($p < 0.001$, Figure 4A); however, both cells had similar nuclear perimeter at one week post-implantation (Figure 4B). Conversely, 40 μm PTS explanted from MyD88KO mice at both one and two weeks express cells with a significantly larger mean nuclear area than nuclei in 40 μm PTS explanted from LysM-Cre:mTmG mice ($p = 0.007$, both; Figure 4A). These results suggest that both pore size and MyD88 signaling influence the nuclear size of the PTS resident cells.

Discussion

In this study, we used HALO® imaging to develop a novel image analysis algorithm that quantifies cell phenotypes and nuclear morphology as a function of PTS pore size. To determine the role of MyD88 signaling in the host response, the cell phenotyping algorithm was applied to 40 μm PTS explanted from MyD88KO mice. Although many image analysis platforms excel in analyzing traditional images, samples containing foreign biomaterials present challenges including resident cells with unique morphology, compensation of biomaterial autofluorescence, and the discrimination of cells from scaffolding material. Thus, the generation of an algorithm specific to biomaterials is essential to accurately phenotype resident cells and further understand the host immune response. Based on our results, HALO® is a novel and comprehensive analytic tool that overcomes specific challenges unique to biomaterial scaffolds.

Within the complex and heterogeneous nature of *in vivo* biomaterial-mediated tissue regeneration, classification of macrophage phenotype and function remains challenging due to the remarkable plasticity of macrophages. Current wound healing literature has heavily relied upon *in vitro* definitions, classifying macrophages as either classically activated “M1” or alternatively activated “M2”. In the classic “M1/M2” paradigm, increased expression of surface marker CD86 is associated as M1-like[24] while CD163 and CD206 expression are associated with an M2-like phenotype[24,25]. However, *in vivo* macrophages are exposed to several polarizing stimuli inducing differential expression of multiple markers that overlap with the classic macrophage phenotypes. Therefore, a kinetic approach by phenotyping with multiple surface markers is necessary to accurately identify *in vivo* macrophage populations within biomaterial scaffolds.

Using the HALO® image analysis algorithm, CD206 was identified as an important surface marker as both the 40 μm PTS implanted in MyD88KO mice and the 100 μm PTS exhibited lower amounts of CD206 compared to the 40 μm PTS implanted in LysM-Cre:mTmG

mice. Although both CD163 and CD206 are polarization markers conventionally associated with a pro-healing phenotype, only CD206 was differentially expressed between pore size and MyD88 experimental groups. Previous transcriptomic data has shown that monocytes upregulate CD206 in 40 μm PTS[12] and give rise to $CD206^+$ wound healing macrophages[26]. Although MyD88 primarily mediates inflammatory cytokine production, the observed change in CD206 expression within the PTS microenvironment suggests additional MyD88-dependent functions associated with $CD206^+$ healing.

Phenotyping of 100 μm PTS showed a greater CD86 pro-inflammatory response suggesting favorable healing in 40 μm PTS. Although no changes in CD3 expression were observed, we have previously demonstrated the role of regulatory T cells in 40 μm PTS healing response[11]. As both macrophages and T cells have been found to play an important regulatory role in the proliferation and remodeling phases of wound healing[27], findings from this study suggest opportunities for further investigation on the application of HALO to T cell subsets within PTS.

Within the scaffolds, the ability to sense different pore sizes appears to result in the nuclear reshaping of resident cells. Investigation of nuclear morphology indicates that 100 μm PTS in LysM-Cre:mTmG mice and 40 μm PTS in MyD88KO mice have significantly larger nuclei than 40 μm PTS in LysM-Cre:mTmG mice. Reports have shown the ability of the nuclear membrane to sense situations of mechanical confinement, and subsequently modulate the cell's migratory behavior within complex 3D microenvironments[28]. Additionally, Lomakin *et al.* have found that when cells are compressed to heights less than 10 μm, the cells actively resist the pressure through a myosin II-mediated contractile response[29]. Since the interconnect diameter of the PTS range from 25–33% of the pore diameter (10–13.3 μm interconnects for 40 μm PTS; 25–33 μm interconnects for 100 μm PTS), the smaller-sized interconnects found in 40 μm PTS may activate a mechanotransduction response leading to the infiltration of cells with morphologically unique nuclei. This suggests that both PTS pore size and MyD88 expression are involved in modulating the nuclear morphology of cellular infiltrates.

Conclusion

In this study, we apply a novel, multiplex HALO® image analysis algorithm to effectively determine cell phenotype in PTS. We were able to acquire single-cell expression and morphological data from explanted 40 μm and 100 μm PTS to identify specific phenotypes and cell populations. At one week post-implantation, 100 μm PTS demonstrate an increase in CD86 expression which is indicative of a pro-inflammatory M1-like phenotype, while at two weeks post-implantation, 40 μm PTS display higher expression of CD206. To investigate the immunomodulatory role of MyD88 signaling in pro-healing 40 μm PTS, 40 μm PTS were subcutaneously implanted in MyD88KO mice. We found that MyD88 signaling is involved in the pro-healing mechanisms seen in 40 μm PTS specifically by a decrease in CD206 expression at both one and two weeks post-implantation in the knock-out animals. Morphological analysis of the nucleus demonstrates that 40 μm PTS features a smaller average nuclear size than cells within 100 μm PTS; however, 40 μm PTS in MyD88KO mice exhibit a nuclear size that closely resembles cells within the 100 μm

PTS. Taken together, our HALO® analysis presents a novel method for cell phenotyping in PTS, and results from this study will allow for the analysis of specific subsets and further characterization of specific biomarkers.

Supplementary Material

Refer to Web version on PubMed Central for supplementary material.

Acknowledgments

Funding for this work was provided by the National Institute of Dental and Craniofacial Research (NIDCR) and the National Institute of General Medical Sciences (NIGMS) (Grant #: NIDCR 5R01DE018701-10 and NIGMS 1R01GM128991-01, respectively). Additionally, this research was supported by the Experimental Histopathology Shared Resource Facility at the Fred Hutch Cancer Research Center for the use of the HALO® image analysis system.

References

1. Caicedo JC et al. Data-analysis strategies for image-based cell profiling. Nature Methods 14, 849–863 (2017). [PubMed: 28858338]
2. Koelzer VH, Sirinukunwattana K, Rittscher J & Mertz KD Precision immunoprofiling by image analysis and artificial intelligence. Virchows Archiv vol. 474 511–522 (2019). [PubMed: 30470933]
3. Vu QD et al. Methods for segmentation and classification of digital microscopy tissue images. Frontiers in Bioengineering and Biotechnology 7, (2019).
4. Hermitte F Biomarkers immune monitoring technology primer: Immunoscore® Colon. Journal for ImmunoTherapy of Cancer 4, (2016).
5. Olsson A et al. Tasquinimod triggers an early change in the polarization of tumor associated macrophages in the tumor microenvironment. Journal for ImmunoTherapy of Cancer 3, (2015).
6. Escuin-Ordinas H et al. Cutaneous wound healing through paradoxical MAPK activation by BRAF inhibitors. Nat Commun 7, 12348 (2016). [PubMed: 27476449]
7. Singh A & Peppas NA Hydrogels and scaffolds for immunomodulation. Advanced materials (Deerfield Beach, Fla.) vol. 26 6530–6541 (2014). [PubMed: 25155610]
8. Vishwakarma A et al. Engineering Immunomodulatory Biomaterials To Tune the Inflammatory Response. Trends in Biotechnology vol. 34 470–482 (2016). [PubMed: 27138899]
9. Madden LR et al. Proangiogenic scaffolds as functional templates for cardiac tissue engineering. Proc Natl Acad Sci U S A 107, 15211–15216 (2010). [PubMed: 20696917]
10. Sussman EM, Halpin MC, Muster J, Moon RT & Ratner BD Porous implants modulate healing and induce shifts in local macrophage polarization in the foreign body reaction. Annals of Biomedical Engineering 42, 1508–1516 (2014). [PubMed: 24248559]
11. Hady TF et al. Uniform 40-μm-pore diameter precision templated scaffolds promote a pro-healing host response by extracellular vesicle immune communication. Journal of Tissue Engineering and Regenerative Medicine (2020) doi:10.1002/term.3160.
12. Chan NR, Hwang B, Ratner BD & Bryers JD Monocytes contribute to a pro-healing response in 40 μm diameter uniform-pore, precision-templated scaffolds. Journal of Tissue Engineering and Regenerative Medicine (2021) doi:10.1002/term.3280.
13. Zhu S et al. Accelerated wound healing by injectable star poly(ethylene glycol)-b-poly(propylene sulfide) scaffolds loaded with poorly water-soluble drugs. Journal of Controlled Release 282, 156–165 (2018). [PubMed: 29751029]
14. Guo C et al. A murine glaucoma model induced by rapid in vivo photopolymerization of hyaluronic acid glycidyl methacrylate. PLoS ONE 13, (2018).
15. Coindre VF, Carleton MM & Sefton M. v. Methacrylic Acid Copolymer Coating Enhances Constructive Remodeling of Polypropylene Mesh by Increasing the Vascular Response. Advanced Healthcare Materials 8, (2019).

16. Li J et al. Tough Composite Hydrogels with High Loading and Local Release of Biological Drugs. Advanced Healthcare Materials 7, (2018).
17. Skinner BM & Johnson EEP Nuclear morphologies: their diversity and functional relevance. Chromosoma vol. 126 195–212 (2017). [PubMed: 27631793]
18. Hou B, Reizis B & DeFranco AL Toll-like Receptors Activate Innate and Adaptive Immunity by using Dendritic Cell-Intrinsic and -Extrinsic Mechanisms. Immunity 29, 272–282 (2008). [PubMed: 18656388]
19. Kawasaki T & Kawai T Toll-like receptor signaling pathways. Frontiers in Immunology vol. 5 (2014).
20. Akira S, Takeda K & Kaisho T Toll-like receptors: critical proteins linking innate and acquired immunity. Nature Immunology 2, 675–680 (2001). [PubMed: 11477402]
21. Amer LD et al. Inflammation via myeloid differentiation primary response gene 88 signaling mediates the fibrotic response to implantable synthetic poly(ethylene glycol) hydrogels. Acta Biomaterialia 100, 105–117 (2019). [PubMed: 31568879]
22. Garg K, Pullen NA, Oskeritzian CA, Ryan JJ & Bowlin GL Macrophage functional polarization (M1/M2) in response to varying fiber and pore dimensions of electrospun scaffolds. Biomaterials 34, 4439–4451 (2013). [PubMed: 23515178]
23. Macedo L et al. Wound healing is impaired in MyD88-deficient mice: A role for MyD88 in the regulation of wound healing by adenosine A2A receptors. American Journal of Pathology 171, 1774–1788 (2007). [PubMed: 17974599]
24. Shapouri-Moghaddam A et al. Macrophage plasticity, polarization, and function in health and disease. Journal of Cellular Physiology vol. 233 6425–6440 (2018).
25. Novak ML & Koh TJ Macrophage phenotypes during tissue repair. Journal of Leukocyte Biology 93, 875–881 (2013). [PubMed: 23505314]
26. Olingy CE et al. Non-classical monocytes are biased progenitors of wound healing macrophages during soft tissue injury. Scientific Reports 7, (2017).
27. Sadtler K et al. Developing a pro-regenerative biomaterial scaffold microenvironment requires T helper 2 cells. Science (1979) 352, 366–370 (2016).
28. Venturini V et al. The nucleus measures shape changes for cellular proprioception to control dynamic cell behavior. Science (1979) 370, (2020).
29. Lomakin AJ et al. The nucleus acts as a ruler tailoring cell responses to spatial constraints. Science (1979) 370, (2020).

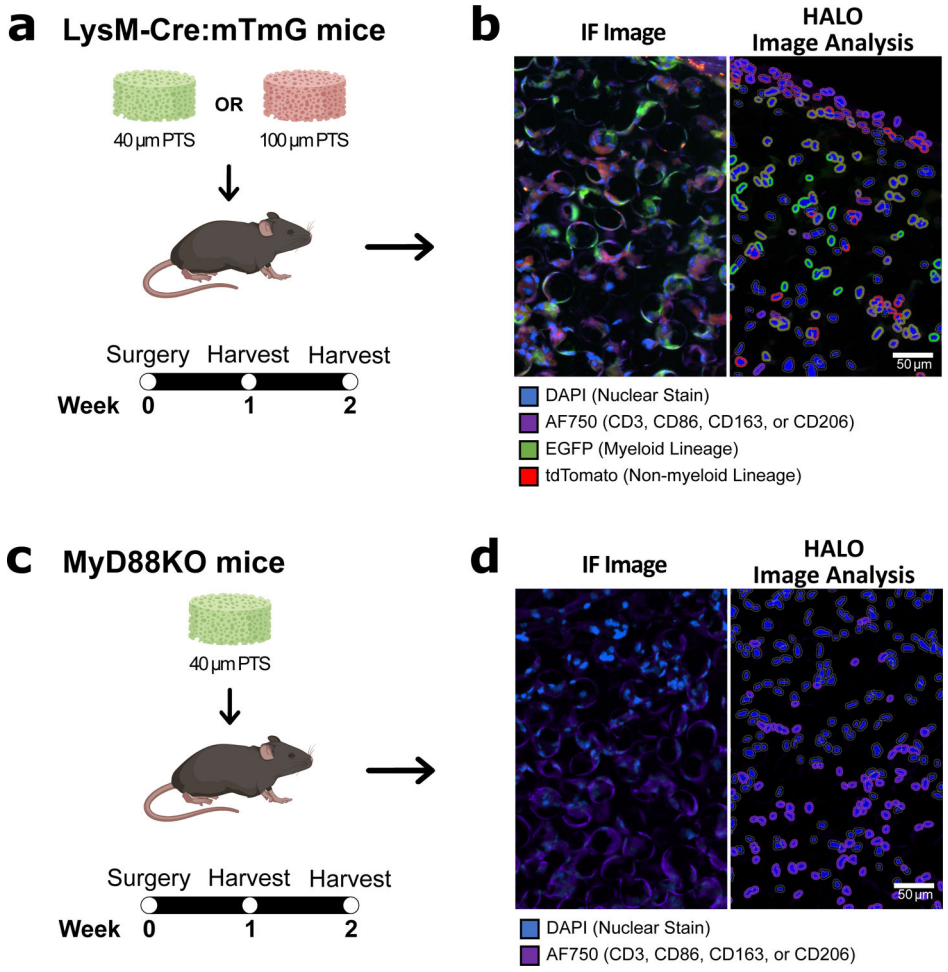

Figure 1:

(**A**) 40 μm PTS or 100 μm PTS were implanted subcutaneously in LysM-Cre:mTmG mice and (**C**) 40 μm PTS were implanted subcutaneously in MyD88KO mice. One and two weeks post-implantation, PTS were excised, cut into 5 μm thick tissue sections, and stained for CD3 (T lymphocytes), CD86 (M1-like macrophages), CD163 (M2-like macrophages), or CD206 (M2-like macrophages) by antibody immunofluorescence labeling. (**B, D**) Immunofluorescent (IF) images of tissue sections collected two weeks post-implantation showing (**left**) the original immunofluorescence images collected by the EVOS imaging system and (**right**) digital renditions generated by the HALO® image analysis software. Scale bar = 50 μm. Colors are blue = nuclei (DAPI), purple = CD3, CD86, CD163, or CD206 (AF750), green = myeloid lineage (EGFP), and red = non-myeloid lineage (tdTomato). HALO® image analysis software was used to quantify positive fluorescence markers in the cytoplasm and nucleus of individual cells. Created with BioRender.com.

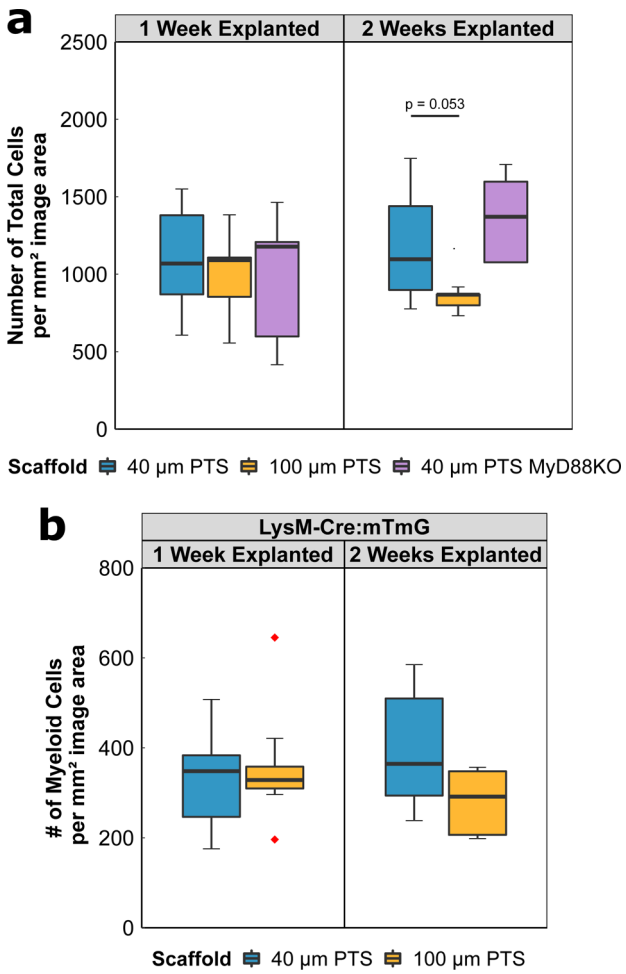

Figure 2:

(**A**) Total number of cells per mm^2 image area from either 40 μm PTS or 100 μm PTS implanted subcutaneously in separate LysM-Cre:mTmG mice, and from 40 μm PTS implanted subcutaneously in MyD88KO mice (40 μm PTS MyD88KO). PTS were explanted at either one week or two weeks post-implantation. (**B**) Number of myeloid cells per mm^2 image area from 40 μm PTS or 100 μm PTS implanted in LysM-Cre:mTmG mice and explanted one week or two weeks post-implantation. 40 μm PTS (n = 10 at one week explanted, n = 6 at two weeks explanted), 100 μm PTS (n = 8 at one week explanted, n = 5 at two weeks explanted), and 40 μm PTS in MyD88KO mice (n = 5 at one week and two weeks explanted). Red diamonds denote values greater than 1.5 × IQR.

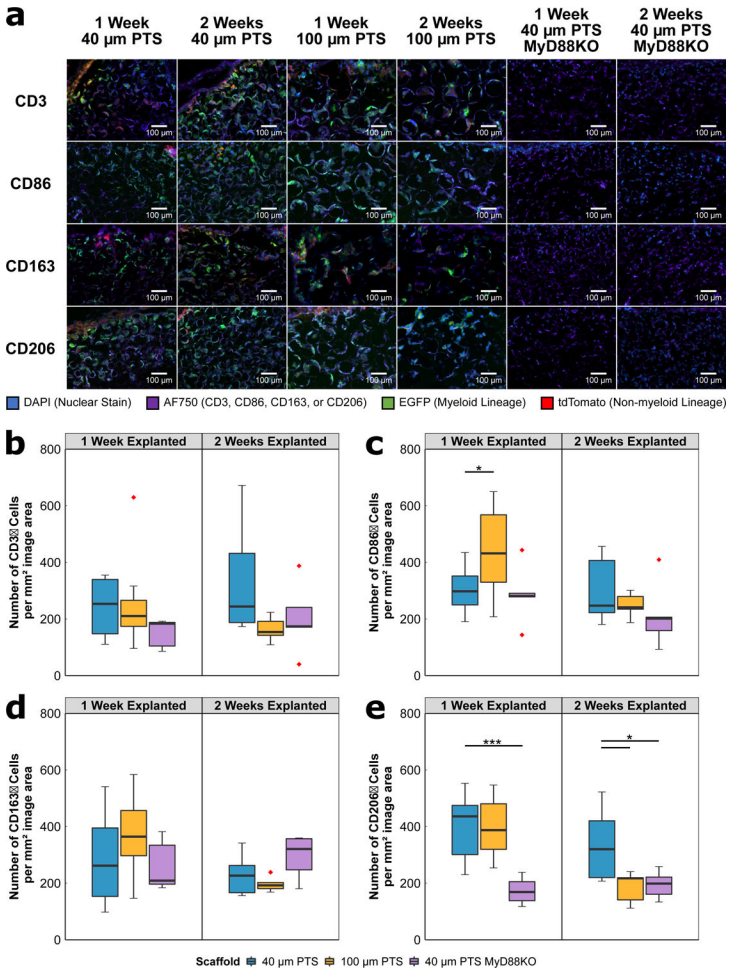

Figure 3:

(**A**) Immunofluorescent images of scaffold tissue sections from either 40 µm PTS or 100 µm PTS implanted subcutaneously in separate LysM-Cre:mTmG mice, and from 40 µm PTS implanted subcutaneously in MyD88KO mice (40 µm PTS MyD88KO). PTS were explanted at either one week or two weeks post-implantation. Colors are blue = nuclei (DAPI), purple = CD3, CD86, CD163, or CD206 (AF750), green = myeloid lineage (EGFP), and red = non-myeloid lineage (tdTomato). HALO® image analysis was performed on single color positive immunofluorescence using a primary antibody specific to (**B**) CD3, (**C**) CD86, (**D**) CD163, and (**E**) CD206, and secondary antibody for AF750. * denotes $p < 0.05$, ** denotes $p < 0.01$, and *** denotes $p < 0.001$. 40 µm PTS (n = 10 at one week explanted, n = 6 at two weeks explanted), 100 µm PTS (n = 8 at one week explanted, n = 5 at two weeks explanted), and 40 µm PTS in MyD88KO mice (n = 5 at one week and two weeks explanted). Red diamonds denote values greater than 1.5 × IQR.

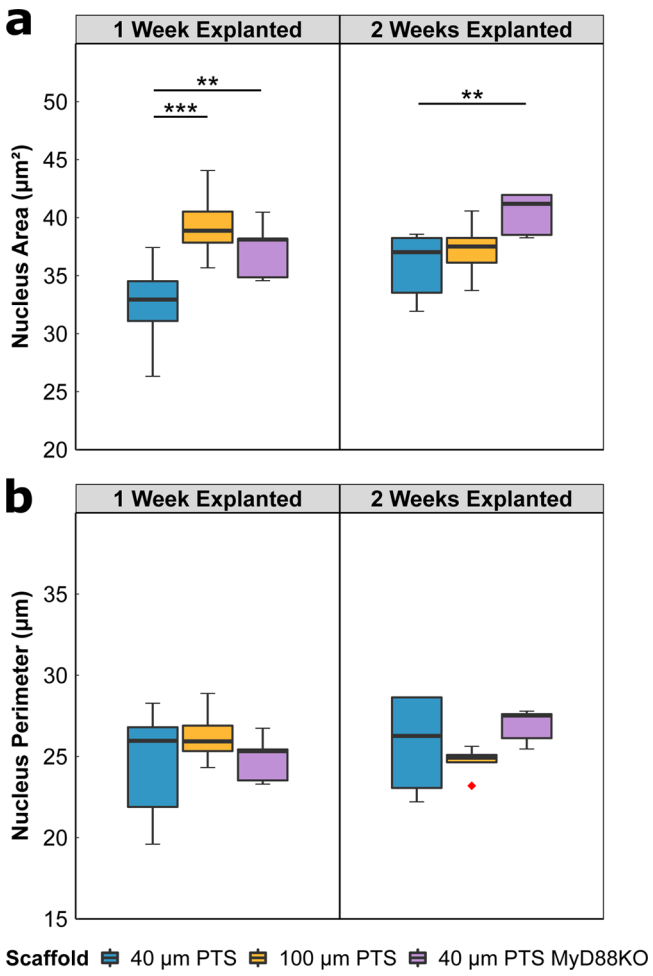

Figure 4:

Nuclear morphology image analysis of scaffold tissue sections from either 40 μm PTS or 100 μm PTS implanted subcutaneously in separate LysM-Cre:mTmG mice, and from 40 μm PTS implanted subcutaneously in MyD88KO mice (40 μm PTS MyD88KO). PTS were explanted at either one week or two weeks post-implantation. Analysis was performed on DAPI-labeled cell nuclei to calculate (**A**) nucleus area and (**B**) nucleus perimeter. * denotes $p < 0.05$, ** denotes $p < 0.01$, and *** denotes $p < 0.001$. 40 μm PTS (n = 10 at one week explanted, n = 6 at two weeks explanted), 100 μm PTS (n = 8 at one week explanted, n = 5 at two weeks explanted), and 40 μm PTS in MyD88KO mice (n = 5 at one week and two weeks explanted). Red diamonds denote values greater than 1.5 × IQR.